JOURNAL OF MATERIALS SCIENCE 30 (1995) 1166–1172

Effects of tensile and compressive stresses on the passive layers formed on a type 302 stainless steel in a normal sulphuric acid bath

F. NAVAÏ
Laboratoire des Matériaux, ISITEM, Université de Nantes, La Chantrerie, C.P. 3023, 44087 Nantes Cedex 03, France

Type 302 stainless steel samples were subjected to a U-bend test in a normal sulphuric acid bath at room temperature. The passive layers which subsequently grew on both sides of the sample, were studied by Auger electron spectroscopy. Each strained sample was immersed and passivated in a sulphuric acid solution under a voltage of +450 mV/SCE and the anodic current density was studied as a function of the immersion time. The results obtained show that the anodic current density is higher for the strained specimens than for the unstrained specimen. Thus, passivation occurs more rapidly for an unstrained sample than for strained samples. There is also clear evidence that the decrease in the anodic current density is more rapid for an elastically strained sample than for a plastically strained one. The influence of the tensile and compressive stresses on the composition of the passive films was studied by comparing the elemental Auger depth profiles. The results obtained show that oxidation is more important on the tensile stressed side than on the compressive stressed one, whether the samples were elastically or plastically strained. Similarly, the width of the region affected by the chromium enrichment was enhanced by tensile straining and reduced by compressive straining, whether the samples were elastically or plastically strained.

1. Introduction

Many papers have reported the study of the effect of mechanical stress on corrosion and depassivation of metal alloys. Representative examples were summarized by France [1] in a paper reporting the results of investigations showed that at passive potentials, deformed steels exhibited greater current densities than those obtained in the annealed steel. Recent experimental results on this subject were given by Desjardins *et al.* [2].

Much attention has been paid to the influence of cold work on the corrosion resistance but, according to the literature, the results appear contradictory. Hawkes *et al.* [3] showed that the cold-work stretching effect on stress corrosion cracking of type 316 stainless steel was deleterious in boiling magnesium chloride solution. Elayaperumal *et al.* [4] studied the effect of cold work on the anodic polarization in normal sulphuric acid (wet corrosion) of type 304 stainless steel cold rolled at room temperature. They found that the effect of a small amount of cold work was insignificant but that attainment of passivity was more difficult when the specimens were highly deformed. Their results were related to the strain-induced martensite which forms the anodic paths when the austenitic stainless steel is cold worked.

Langevoort *et al.* [5] studied the oxidation behaviour at elevated temperature (dry corrosion) of drawn AISI 304, AISI 321 and Incoloy 800 H stainless steels, and found that types 304 and 321 show same oxidation behaviour with a decreasing corrosion resistance with increasing deformation. Furthermore, they believe that a deformed specimen could present a better corrosion resistance at high temperature than does an undeformed specimen, if the specimen was drawn below the temperature $M_d = 340$ K. Because the martensite formed within the austenic matrix [6] is body centred cubic, it will have a higher rate of diffusion for chromium. Consequently, the passive film will be richer in chromium and thus more protective. On the other hand, it was noticed that on increasing the deformation, the faster the oxidation of Incoloy 800 H became, because of the large number of defects induced by the plastic deformation in the oxide.

Pednekar and Smialowska [7] in their work on the sensitization of type 304 stainless steel showed that small amounts of prior cold work should induce a large increase in the dislocation density in the grain-boundary region, and sharply enhance the susceptibility to subsequent sensitization. Large amounts of cold work, prior to sensitization, result in the complete absence of sensitization after several hours treatment at 660 °C. Similar results were obtained by Briant and Ritter [8] for the stress corrosion susceptibility of type 304 stainless steel. Charbonnier [9] indicated that

0022–2461

although the literature contained many references showing that small amounts of cold work (less than ~ 20%) decreased the ability to passivate the austenitic steels [10], there were some indications showing that the opposite effects could be observed [11]. This is, for instance, the case for cold rolling, extrusion and sandblasting, which produce compressive residual stresses and enhance the samples resistance to aggressive baths.

The passivity phenomenon resulting from the protective film formation and the basic models was discussed by Scully [12]. The models are supported by information given by physico-chemical analysis techniques such as electron spectroscopy for chemical analysis, Auger electron spectroscopy, ellipsometry, infrared spectroscopy [13–16]. For instance, Okamoto [13] considered that the corrosion resistance of the passive steel is controlled by the nature of the passive film. The prime stress effect on passive films is to produce fresh metal areas disbonded from the passive film through the emergence of slip steps. Such a mechanism was widely discussed in relation to the role of oxide films in stress corrosion cracking in metals [17]. It can be thought that because compressive stresses tend to close the cracks and reduce the real contact surface of the alloy with its environment, they should have a beneficial effect on the stress corrosion resistance of the metallic alloys.

The literature is very poor concerning the effect of compressive stress on the behaviour of stainless steels. Therefore, the original aim of this work was to determine whether the passive film properties developed on both sides of a U-bend specimen were different according to the tensile or compressive nature of the stress.

2. Experimental procedure

2.1. Base material

The rectangular specimens, 100 mm long, 7 mm wide and 0.25 mm thick, used in the present study were cut from a type 302 stainless steel sheet. The longitudinal axes of the samples were orientated parallel to the prior rolling direction of the sheet. The nominal composition of the base material is given in Table I. As given by the supplier Goodfellow, the principal properties of the type 302 "Hard" stainless steel are: Young's elastic modulus 190 GPa, hardness 190 Brinell. Some other mechanical properties were measured: ultimate tensile strength 1450 MPa, and 0.2% offset yield strength about ~ 1000 MPa.

2.2. Surface pretreatment

The test specimens received the following initial preparation. They were washed with soap, rinsed with water, and ultrasonically degreased in an acetone bath. They were then electropolished at 35 °C, for 150 s, in a bath prepared by mixing 15% analytical reagent grade sulphuric acid (R.P. Normapur, 95% minimum, $d = 1.83$) and 85% analytical reagent grade orthophosphoric acid (R.P. Normapur, 85% minimum, $d = 1.70$). During the entire electropolishing treatment the current density was maintained at a constant value of 1 A cm^{-2}. The samples were then rinsed in demineralized water and finally dried in a hot-air flow.

TABLE I Chemical composition of the base material (wt %)

Cr	Ni	Mn	C	S	P	Fe
17–20	7–11	< 2	< 0.16	< 0.03	< 0.045	Balance

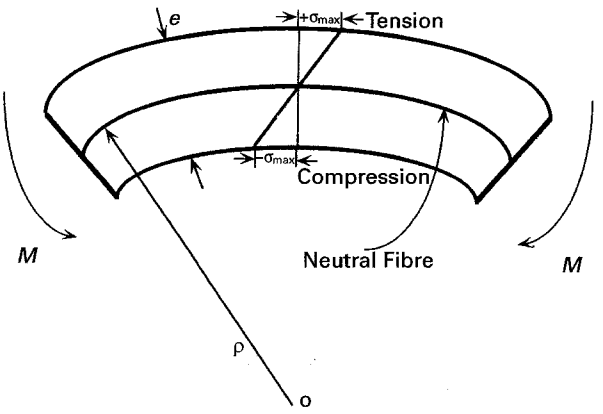

Figure 1 The tensile and compressive stress distribution on the sides of the U-bend specimen.

2.3. Mechanical stressing

After surface treatment and before immersing in the acidic bath, the samples were bent into a U-shape using a mechanical system. Two different strains were given to the samples. Some of the samples, denoted E, were bowed at a diameter of 36 mm giving a radius of curvature $\rho = 18 \pm 1$ mm (see Fig. 1). Under such circumstances, these specimens almost recovered their initial form when the applied stress was suppressed, so that their plastic deformation was very small, inferior to 0.2%, the offset yield strength. The other strained samples, denoted P, were bowed at a diameter of 8 mm. They remained permanently deformed when the applied stress was suppressed. However, some unstrained samples denoted R and R′ were studied as reference specimens.

The strain, ε, on the superficial layers can be calculated from the following relationship (see Fig. 1)

$$\varepsilon = e/2\rho \quad (1)$$

where e (= 0.22 mm) is the specimen thickness after electropolishing, and ρ is its radius of curvature, thus $\varepsilon = 0.11/\rho$. Knowing the stress–strain curve plotted for type 302 stainless steel, the stress in the outer layers can be determined.

Table II indicates the maximum stress in the outer layers of the U-bend samples. However, if a compressive residual stress exists on the surface, the stress distribution will follow an algebraic summation of the external bending stresses and the residual stresses. This, for a very thin oxide film, is about 50 MPa [17].

TABLE II Comparison of stress and strain of the U-bend specimens

Samples	Radius of curvature (mm)	Strain (%)	Maximum stress estimation (MPa)
R	∞	–	Residual
E	18 ± 1	0.6	900
P	4 ± 1	2.7	1400

Thus, the peak tensile stress is displaced to a point in the interior of the specimen.

After receiving surface treatment and before immersion in the acidic bath, the samples were mechanically bent into a U-shape.

2.4. Dipping attack

After straining, the samples were quickly immersed in 1N H_2SO_4 solution at pH zero and the transient passivation behaviour of the samples was studied as a function of immersion time.

In order to prevent the formation of the thin oxide layer on the sample surface between the end of the mechanical straining and its introduction into the bath, the sample was first cathodically pre-treated at about -550 mV with respect to the reference electrode. The cathodization was stopped when the current density reached an approximate value of 1 mA cm^{-2}, and then anodization treatment was begun.

3. Results and discussion

3.1. Preliminary study

In order to study the role of the surface morphology and roughness on the passive layer formed on type 302 stainless steel, two specimens were prepared. The first one, R, was only electropolished before passivation. The second specimen, R′, was ground with 1200 grit SiC emery before electrochemical polishing and passivation. The R samples, which were not mechanically polished before electrochemical polishing, presented a very smooth surface, whereas, for the R′ samples, the surface was rough and many marks were clearly visible. In spite of these visual differences on the surface morphologies, no important differences were observed in the depth profile composition obtained by Auger electron spectroscopy (AES) coupled with Ar^+ ion sputtering (See Fig. 2).

3.2. Polarization curves

In order to determine the passivation potential domain, anodic potentiodynamic measurements, giving the electrochemical current intensity dependence as a potential function, were made on the reference sample at a scanning rate of 100 mV min^{-1}. These measurements were conducted by placing the used samples as the working electrode, in the presence of a platinum cathode as the counter-electrode and a saturated calomel reference electrode in the electrolyte bath. All sample potentials were measured against

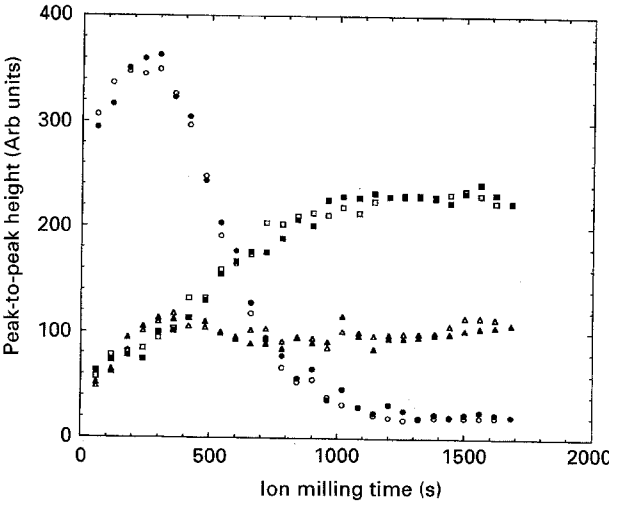

Figure 2 Comparison of the depth dependence of the (○, ●) oxygen, (□, ■) iron and (△, ▲) chromium Auger line heights. Before passivation, the sample was either (●, ■, ▲) mechanically and electrochemically polished (R′) or (○, □, △) only electrochemically polished (R).

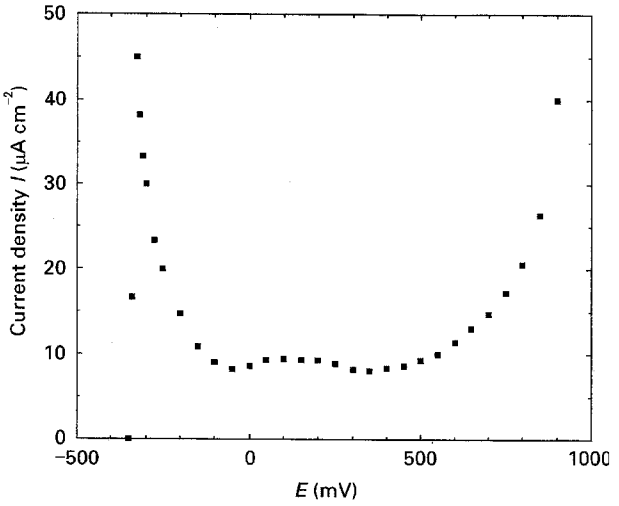

Figure 3 Potentiodynamic polarization curve for the type 302 stainless steel in 1 N sulphuric acid solution. Sample potentials were measured against the saturated calomel electrode (SCE).

the saturated calomel electrode (SCE). The results of the present investigation are plotted in Fig. 3 showing that the passivation domain ranges from about -100 mV to nearly $+900$ mV with a minimum current of 10 μA at about $+450$ mV/SCE. It is worth noting that the general shape of the plot is similar to that described earlier for chromium [13]. The 450 mV value for which the anodic current is minimum was chosen as an electrode potential in the subsequent potentiostatic tests to study the passivation kinetics of the strained samples.

3.3. Passivation kinetics of the strained samples

Each strained sample was immersed in a sulphuric acid solution under a voltage of $+450$ mV/SCE and the anodic current density was studied as a function of immersion time. The results shown in Fig. 4 are

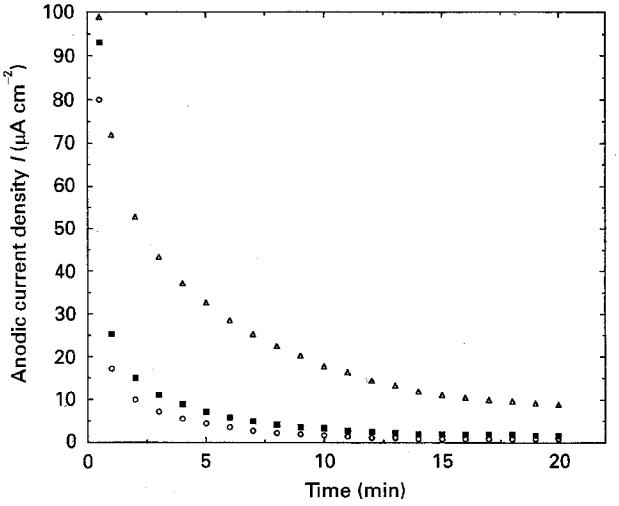

Figure 4 Current density–time curves for (○) R, (■) E and (△) P samples in 1 N sulphuric acid solution.

compared with those obtained for the reference sample. We can see that the anodic current density and the dissolution rate is higher for E and P samples than for R samples. The anodic current density is the sum of the dissolution current of the passive film and the passivation current, and it is a linear function of percentage strain [18]. Consequently, passivation occurs more quickly for the reference sample than for the strained specimens. There is also clear evidence that the decrease in the anodic current density is faster for the elastically strained E sample than for the plastically strained one. For instance, after 10 min immersion in the sulphuric acid bath, the anodic current density was about 3, 4 and 20 $\mu A\,cm^{-2}$ for the reference sample, the elastically strained sample and the plastically strained one, respectively.

3.4. Physico-chemical analyses

Passivated substrate surface observations were made by SEM and the depth profiles composition measurements were carried out by AES. In order to compare observations the measurements were made on both the compressive and tensile strained surfaces. The samples were kept in the passivation bath for 20 min, as mentioned previously, to ensure that a sufficient passivation and a stable oxide film formed on the specimens.

Fig. 5 shows the surface morphologies obtained for the plastically strained P sample. The tensile strained surface, Fig. 5a, presents a very coarse morphology revealing rather strong attack. The surface appears rather rough with many marked hills and valleys, and dirty with many black spots. On the contrary, the compressive strained surface, Fig. 5b, appears cleaner. Furthermore, numerous slip steps are visible. They appeared more or less parallel, although having a given orientation for a given grain. Consequently, the patterns developed on grains give some indication of the grain-boundary shape. No attempt was made to determine the eventual structural changes likely to occur with increasing strain. The E sample

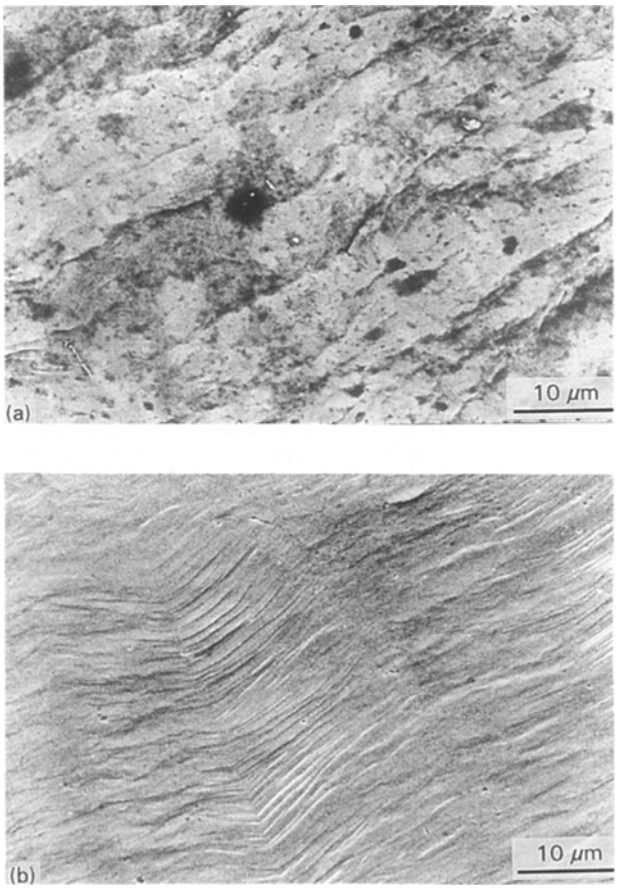

Figure 5 Scanning electron micrographs showing the effects of the passivation treatment on (a) the tensile strained side, and (b) the compressive strained side of a U-bend type 302 stainless steel (P specimen) in 1 N sulphuric acid solution.

morphology surfaces are quite similar to that of the reference sample, irrespective of the compressive or tensile nature of the strain, and the straining preparation will not be shown here.

For the AES analysis, separate freshly prepared samples were used for compositional depth profile analysis. After passivation, the samples were taken from the bath, immediately rinsed in water, dried and introduced into an Auger electron spectrometer. The elemental depth profiling was obtained from a series of repeated cycles of argon ion abrasion; afterwards Auger analyses were plotted from peak-to-peak heights of the principal Auger lines against the ion milling time, as in Fig. 2a and b. Each ion abrasion time was 60 s long, corresponding to an elimination thickness of about 0.48 nm on a sample of silicon. No attempt was made to determine the real elemental concentration, as this could be determined from the sensitivity factors. The results obtained are shown in Fig. 6 and can be analysed as follows.

In Auger spectra, the substrate is characterized principally by the iron Auger lines at 598, 651 and 703 eV, the chromium lines at 489 and 529 eV and the nickel lines at 716, 783 and 848 eV. Similarly, the passive film is characterized by the 510 eV oxygen line, 272 eV carbon characteristic line, and sulphur by its characteristic line at 152 eV. The peak-to-peak heights of the principal Auger lines (the 703 eV Fe line, the

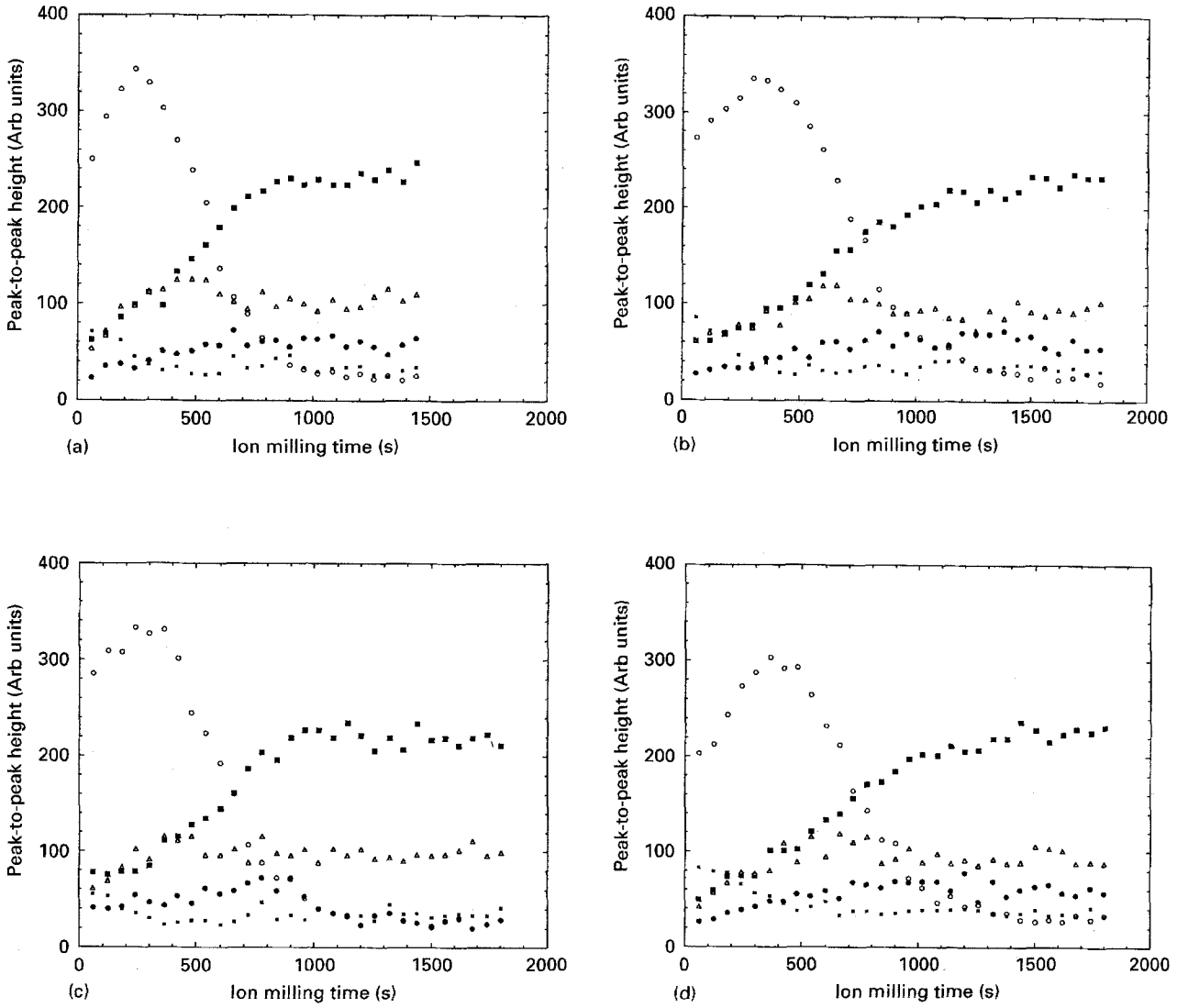

Figure 6 AES depth concentration profiles of the passive film formed on type 302 steel specimens in 1 NH_2SO_4 solution. The profiles were measured on (a) the compressive strained side of the E sample, (b) the tensile strained side of the same sample, (c) the compressive strained side of the P sample, and (d) the tensile strained side of the same sample: (○) O, (■) Fe, (△) Cr, (●) Ni, (▪) C.

529 eV Cr line, the 848 eV Ni line, the 510 eV O line, and the 272 eV C line) have been plotted against the ion milling time in Fig. 2.

The most noticeable fact is that the apparent width of the passive film as illustrated by the oxygen line depth dependence, is the same irrespective of the mode of preparation. This is clearly shown in Fig. 2, which presents simultaneously for the two different surface preparations, the change in the heights of the oxygen, iron and chromium Auger peaks as a function of ion milling time in the Auger spectrometer (nickel, carbon and sulphur are not reported for clarity).

The concentration of sulphur in the alloy is very low ($< 0.03\%$) and does not seem to influence significantly the passive layer. In fact, it is observed that the sulphur Augur line at 152 eV is confined in depth to a very narrow domain near the surface. This can be interpreted as being principally due to bath contamination and sulphate ion absorption at the surface which is much more unlikely than a surface segregation from the bulk, which occurs at elevated temperature of about 600–800 °C. However, the sulphur line intensity is somewhat greater on the tensile strained surface side than on the compressive strained side.

The presence of the 272 eV C line all along the depth profile plot, shows that carbon is detected in each face, the bulk alloy concentration of carbon is less than 0.16%. As seen in Fig. 6a–d, the 272 eV carbon Auger line decreases rapidly in strength with increasing depth. This can be explained by the presence of carbon on the steel surfaces resulting from an external contamination produced by exposure to CO_2 from the atmosphere rather than the nucleation and growth of carbide. However, it can be observed that the carbon line intensity in the outer layers is somewhat greater on the tensile strained surfaces than it is on the compressive strained one or on the reference sample.

It was observed that, in general, the passive film region was relatively enriched in chromium and only slightly in nickel. Fig. 6a–d show that the chromium-enriched layer is followed by a depleted region, because of chromium migration to the passive film. This occurred only at great depth when the chromium content reaches its bulk value. Fig. 7a, b shows the Auger peak height ratio changes of

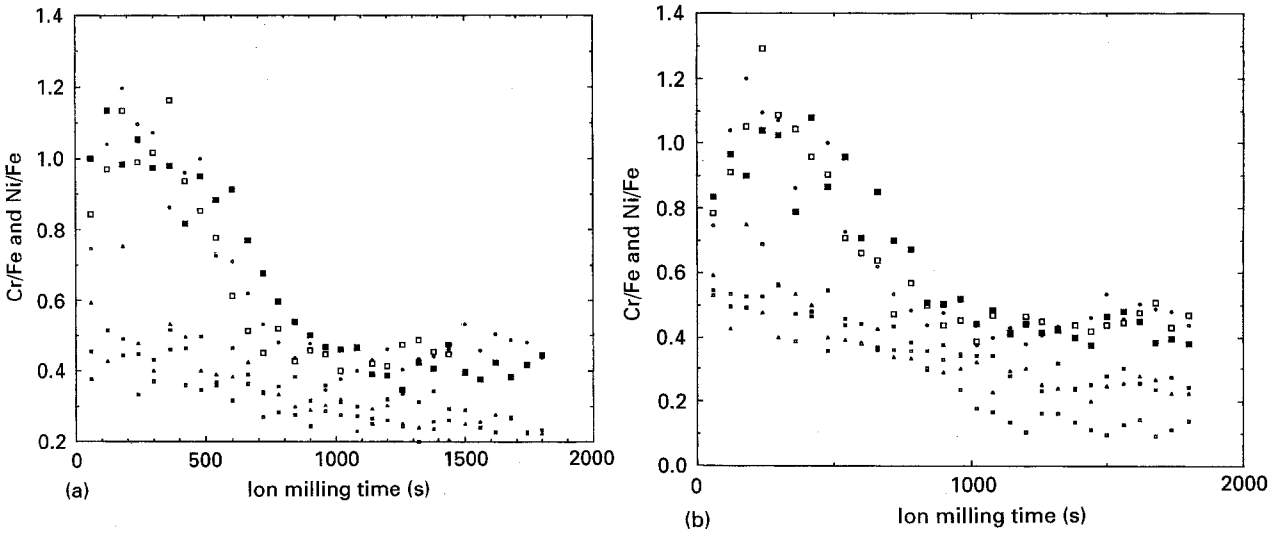

Figure 7 Ratios of the Auger peak heights (○, □, ■) Cr(529 eV)/Fe(703 eV) and (▲, □, ■) (Ni(848 eV)/Fe(703 eV) as a function of the ion milling time, (a) for the (□, □) E compressive (■, ▲) E tensile and (○, ▲) R samples, (b) for the (□, □) P compressive, (■, ■) P tensile and (○, ▲) R samples.

Cr(529 eV)/Fe(703 eV) and Ni(848 eV)/Fe(703 eV) of both samples as a function of the ion milling time. The Cr(529 eV)/Fe(703 eV) pronounced dependence ratio indicates that there is also a selective enrichment of chromium, because of both chromium migration towards the oxide film and an eventual preferential dissolution of iron.

The width of the region affected by the chromium enrichment depends on the tensile or compressive nature of the strain. More precisely, the width of the affected region is greater on the tensile strained surface than it is on the compressive strained one, as shown in Fig. 7a for the sample E and despite the fact that the plots are not very smooth. In fact, the width of the affected region is approximately associated with the passive film thickness. We can conclude, at least in the present case, that the film thickness is more enhanced under tensile straining and reduced under compressive straining. A similar effect was observed for sample P, but probably because of an increase in the substrate surface roughness, the plots appear somewhat rougher than they were in R (see Fig. 7b).

The Ni(848 eV)/Fe(703 eV) ratio depth profile shows a slight decrease from the surface to the bulk sample, suggesting that there is also a weak interaction between oxygen and nickel in the passive film area. Similar results have been described previously by Okamoto [13] for the same case.

A very interesting result arises from a comparison of the elemental depth profiles obtained from the strained and unstrained surfaces. In fact, strong evidence of film thickness enhancement is provided in Fig. 8, showing the peak-to-peak height plots of the 510 oxygen line against the ion milling time. It is observed that the passive layer is richer in oxygen on the tensile strained surfaces than it is on the unstrained sample surfaces and thicker on the latter than it is on the compressive strained surfaces.

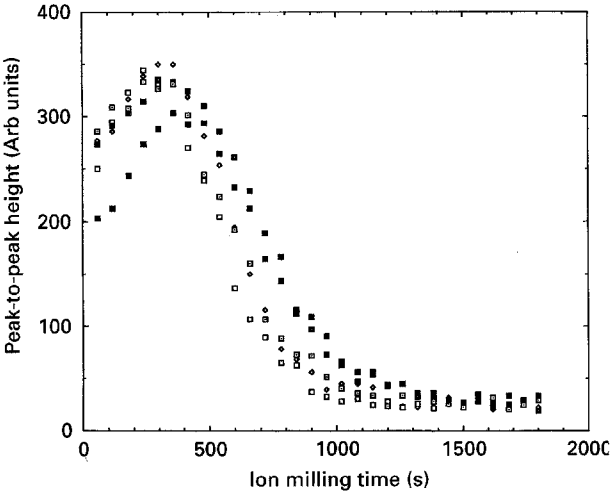

Figure 8 AES depth profiles for oxygen showing the effect of straining on the passive film width, for (◇) the R sample and (□, ⊡) compressive and (◘, ■) tensile strained sides of both E (□, ◘) and P (⊡, ■) samples.

From a comparison of the elemental depth profiles obtained on the elastically and the plastically strained samples (Fig. 8), it can be seen that, for a compressive strain, the passive layer thickness appears slightly enhanced in the plastically strained sample. On the contrary, for a tensile strain, the passive film, as described by the intensity of the oxygen line, appears narrower and less compact in the plastically strained sample. This observation is in agreement with the results obtained for the time–current density dependence which show that the passive film is formed quickly in the elastically strained sample E than it is in the plastically strained one, P (Fig. 4). This result is somewhat unexpected, in that the slip steps are preferential pitting spots which should favour surface attack in the sulphuric acid bath.

In order to study the reproducibility phenomena we repeated the same experiment for various radii of

curvature and for different degrees of cold working. We noticed that the obtained results were always the same. Thus, the tensile strained surface was always richer in oxygen than the compressive strained one. The increase in the relative depth ratios of the oxide thickness

$$100\ (d_{\text{tens.}} - d_{\text{comp.}})/d_{\text{comp.}} \qquad (2)$$

where $d_{\text{tens.}}$ and $d_{\text{comp.}}$ are the average thicknesses of oxide films formed on tensile and compressive sides of specimen, respectively, vary from 10%–25%.

These results can be explained qualitatively as follows: when oxidation occurs the internal stress can arise from the difference between the original volume of the metal atom and the volume of oxide it forms; this latter volume divided by the former is termed the Pilling–Bedworth ratio. The Pilling–Bedworth ratio is more than 1 for the oxides formed on the surface of stainless steels. Consequently, the formation of oxide will lead to the generation of compressive stress in the oxide and tensile stress in the substrate. Now, when an external tensile stress is applied, the new oxide can form, for instance, at grain boundaries, which relieves stress rather than creates it. It is also possible that the new oxide forms at cracks or open pores [19] in the oxide scale. However, when a specimen is under an external compressive stress, this tends to close the cracks and the pores, reducing the real area of the specimen in contact with the solution. Furthermore, in this case the formation of oxide creates and augments the residual compressive stress reducing the oxidation kinetic.

4. Conclusions

The 302 stainless steel type samples were subjected to a U-bend test in a normal sulphuric acid bath at room temperature and passive layers grown on both sides of the samples deformed in the U-form were studied by Auger electron spectroscopy. Each strained sample was immersed in sulphuric acid solution and passivated under a voltage of + 450 mV/SCE and the anodic current density was studied as a function of immersion time. The results obtained in this work allow the following conclusions to be drawn.

1. The anodic current density is higher for the strained specimens than for the unstrained specimen. Furthermore, the decrease in the anodic current density is faster for an elastically strained sample (plastic strain $\leqslant 0.2\%$) than for a plastically strained one.

2. The protective passive layer formed more rapidly on an unstrained sample than on strained samples. However, the oxide film formed on a compressive stressed surface appears more compact.

3. The passive film is richer in oxygen (thicker) on the tensile stressed surface than on the compressive stressed one, whether the samples were elastically or plastically strained. Furthermore, the thickness of the oxide film developed on an unstrained sample was found to be intermediate between those of the strained sample films, but more analogous to the oxide film thickness formed on the compressive stressed side.

4. The width of the area affected by the enrichment in chromium was found to be enhanced by the effect of tensile straining and to be reduced under compressive straining, whether the samples were elastically or plastically strained.

Acknowledgement

The author thanks the Auger team of Ecole Centrale de Nantes for Auger Electron Spectroscopy analyses.

References

1. W. D. FRANCE Jr, *Corr. NACE* **26** (1970) 189.
2. D. DESJARDINS, M. PUIGGALI, L. AJANA and M. C. PETIT, in Actes du 7ème Congrès Européen de corrosion", Nice, November 1985.
3. H. P. HAWKES, F. H. BECK and M. G. FONTANA, *Corr. NACE* **9** (1963) 247t.
4. K. ELAYAPERUMAL, P. K. DE and J. BALACHANDRA, *ibid.* **28** (1972) 269.
5. J. C. LANGEVOORT, T. FRANSEN and P. J. GELLINGS, *Werkst. Korr.* **34** (1983) 50.
6. A. CIGADA, *Corr. Sci.* **22** (1982) 559.
7. S. PEDNEKAR and S. SMIAOLOWSKA, *Corr. NACE* **36** (1980) 565.
8. C. L. BRIANT and A. M. RITTER, *Scripta metall.* **13** (1979) 177.
9. J. C. CHARBONNIER, *Mém. Etudes Sci. Rev. Métall.* **3** (1981) 121.
10. H. L. LOGAN, and M. J. McBEE, Materials Research and Standards, ASTM Special Technical Pulication 264, p. 38, Case History No. 49 (Amercian Soceity for Testing and Materials, Philadelphia, PA, 1961).
11. T. P. HOAR and J. G. HINES, *J. Iron Steel Inst.* **182** (1956) 124.
12. J. C. SCULLY, in "Atomistics of fracture", edited by R. M. Latanision and J. R. Pickens, NATO Conference seris, series VI: Materials Science (Plenum Press, New York, London, (1983) p. 637.
13. G. OKAMOTO, *Corr. Sci.* **13** (1973) 471.
14. D. M. KOLB, *J. Vac. Sci. Technol.* **A4** (1986) 1294.
15. G. LORAND, F. BASILE, M. DA CUNHA BELO and J. P. LANGERON, *Surf. Interface Anal.* **12** (1988) 428.
16. C. LEMAITRE, *Mét. Corr. Ind.* **723–724** (1985) 331.
17. N. SATO, *Electrochem. Acta* **16** (1971) 1683.
18. T. P. HOAR and J. R. GALVELLE, *Corr. Sci.* **10** (1970) 211.
19. W. JAENICKE, S. LEISTIKOW and A. STADLER, *J. Electrochem. Soc.* **111** (1964) 1031.

Received 17 May
and accepted 5 September 1994